Materials and Design 133 (2017) 444–454

Contents lists available at ScienceDirect

Materials and Design

journal homepage: www.elsevier.com/locate/matdes

Flax fiber-reinforced composite lattice cores: A low-cost and recyclable approach

Jun Xu [a,b,c,d], Xiang Gao [a,b], Chong Zhang [b,e], Sha Yin [a,b,c,*]

[a] Department of Automotive Engineering, School of Transportation Science and Engineering, Beihang University, Beijing 100191, China
[b] Advanced Vehicle Research Center (AVRC), Beihang University, Beijing 100191, China
[c] State Key Laboratory for Strength and Vibration of Mechanical Structures, School of Aerospace Engineering, Xi'an Jiaotong University, Xi'an 710049, China
[d] State Key Laboratory for Automotive Safety and Energy, Tsinghua University, Beijing 100084, China
[e] Department of Aircraft Airworthiness Engineering, School of Transportation Science and Engineering, Beihang University, Beijing 100191, China

HIGHLIGHTS

- Flax fiber reinforced lattice materials were designed, fabricated with a low-cost approach.
- Lattice cores with flax fiber composites and foam sandwich struts were tested and compared.
- An orthotropic constitutive model was proposed and deduced with lattice geometry and material property.
- Sensitivity of processing defects was studied by simulation which would help the optimal design of lattice geometry.
- A property-cost chart was created and flax fiber reinforced lattice cores filled the low-cost gap area.

GRAPHICAL ABSTRACT

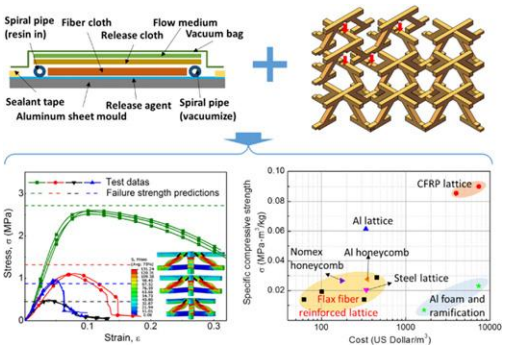

ARTICLE INFO

Article history:
Received 10 June 2017
Received in revised form 27 July 2017
Accepted 28 July 2017
Available online 31 July 2017

Keywords:
Flax fiber
Lattice material
Constitutive model
Mechanical property
Defect sensitivity
Cost

ABSTRACT

Lightweight, low cost, and recyclability are priorities in various material selections. In this study, flax fiber-reinforced lattice cores with redesigned lattice geometry were developed and manufactured by vacuum-assisted resin infusion and slot assembly method. An orthotropic constitutive model of the redesigned lattice cores was proposed, and the elastic compliance matrix was expressed with lattice geometry and properties of parent materials. Then, lattice structures with composites and foam sandwich trusses were fabricated and compressed, respectively. Specific nominal stiffness and strength values of the latter were approximately 1.5× and 2× those of their monolithic counterparts. Subsequently, mechanical property sensitivity of defects formed during processing was simulated, and the results provided additional insights to optimize the lattice design. A property-cost chart was specially created, and flax fiber-reinforced lattice cores proved to be promising candidates for automotive lightweight industry because of their economy and recyclability.

1. Introduction

Energy and environment sustainability are currently the top priorities in the society such that lightweight, low cost and recyclability are the most intriguing material properties for various large-scale industries,

* Corresponding author at: Department of Automotive Engineering, School of Transportation Science and Engineering, Beihang University, Beijing 100191, China.
E-mail address: shayin@buaa.edu.cn (S. Yin).

http://dx.doi.org/10.1016/j.matdes.2017.07.066
0264-1275/

Nomenclature

l_1	strut length
l_2	length between two inclined struts at the pyramidal node
l_3	length of horizontal trusses
ω	inclination angle between the struts and the horizontal truss of the unit cell
b	width
t	thickness
t_f	thickness of face sheet
t_c	thickness of foam core
ρ_{equ}	equivalent density
ρ_f	density of face sheet
ρ_c	density of foam core
ρ_s	density of parent material of foam
E_c	compressive modulus of foam
G_c	shearing modulus of foam
C_v	material cost per volume
E_Z	through-thickness compressive modulus
G_{XZ}	through-thickness shear modulus
A_S	nominal cross section area of the unit cell
ε	strain
σ_f	crush strength of face sheet
E_f	compressive modulus of face sheet
E_s	Young's modulus of parent material of foam
σ_s	compressive strength of parent material of foam
ϕ	volume ratio of cell wall materials and the unit cell of foam
δ	displacement
F_a	axial force
F_s	shear force
A	compressive stiffness
D	bending stiffness
S	shearing stiffness
τ_c	shearing strength of foam
c_{kg}	material cost per kg
E_X	in-plane compressive modulus
υ	Poisson's ratio

e.g., automotive and aerospace industries [1,2]. Thus, lightweight design, including light material selection and structural optimization, has become a hot industrial topic [3,4]. Structural optimization has certain limits to considerably and satisfactorily reduce weight. Thus, new material substitutions and applications have attracted much attention. Lightweight attribute is achieved by traditional methods through the use of low-density alternative materials (e.g., high-strength steel, lightweight alloys, and emerging composite materials) with high mechanical properties, which are clearly indicated in the Ashby Chart [5]. Environment-friendly natural fiber-reinforced composite materials have gained promising applications because of their attractive properties, such as low cost, degradability, high specific strength and stiffness, and thermal and acoustic insulation. Thus, natural fibers have attracted special attention.

Cellular materials, such as metal foam, aluminum honeycomb, and lattice structures, are highly popular in mechanical structures [6]. The lattice structure is a material formed by the ordered arrangement of a certain unit cell [7,8]. Studies on metallic lattice structure have been conducted using various fabrication approaches [9] and the mechanical properties of a structure [10,11]. Xiao et al. [12] fabricated Ti-Al-4V metallic lattice materials by 3D printing and then studied the mechanical performance of the fabricated materials. Composite lattice structure has become available with even higher strength-to-density ratio, thermal shielding, and corrosion resistance. Russell et al. [13] developed a kind of carbon fiber-reinforced composite honeycomb core structure by slot insertion approach and tested the quasistatic compression and shearing and dynamic compression properties. Finnegan et al. [9] first developed a water cutting and slot insertion approach to fabricate composite pyramidal lattice structure, and the mechanical properties of the structure were tested. Liang et al. [14] studied the shear response of an octet-truss lattice structure fabricated with carbon fiber composite. Liu et al. studied the energy absorption characteristics of hollow microlattice structures under quasistatic [15] and dynamic [16] condition. Yin et al. [17–21] examined the out-of-plane compression behavior of several types of carbon fiber-reinforced composite lattice structure, such as structures with hollow composite trusses, hybrid trusses, and hierarchical trusses. Hierarchical composite lattice cores with foam sandwich struts were found to have comparable mechanical properties with optimized hollow lattice truss materials, which showed excellent structural efficiency with relatively simple fabrication method. Moreover, sandwich structures with several traditional lattice cores (e.g. pyramidal and tetrahedral) often fail by debonding at the core-face sheet interface in shear or bend loading, which is attributed to the small connecting area at the interface [22].

However, few studies on natural fiber as reinforced composite lattice structure have been conducted. Intuitively, natural fiber-reinforced composite lattice material would present not only relatively high strength-density ratio but also a recyclable resolution to current artificial fiber reinforced material. Flax fibers are one of the promising candidates among available biofibers because of their unique properties, low cost, health advantages and environmental impact. Several related works on flax fibers have already been performed [23]. Thus, in this study, flax fiber-reinforced composite lattice materials were designed with additional horizontal beams of variable length for optimized overall mechanical properties. Then, the materials were fabricated via a low-cost vacuum assisted resin infusion (VARI) and slot assembly process. Monolithic lattice cores with pure composites trusses and hierarchical ones with foam sandwich trusses were fabricated and through-thickness compressed, respectively. Elastic constitutive models expressing stress-strain relationship and prediction models of compressive strength were developed theoretically. In addition, sensitivity of defects induced during fabrication was discussed by simulation.

2. Experimental

2.1. Fabrication

2.1.1. Raw material selection

Flax fiber plain weave fabrics (purchased from Linyi City, Shandong Province, China) were selected as reinforcement phase of composites. Fabric morphology was observed using an optical microscope with 20× magnification (Fig. 1a). The diameters of tows in the fabrics vary approximately from 0.6 mm to 1.5 mm. The area density of the fabric was measured to be approximately 0.23 kg/m^2.

An epoxy resin system (LY1564/Aradur22962, Huntsman) was selected to fabricate the composites, because thermoset polymers can be cured at temperatures well within the safe range for natural fibers. Although the thermoset composites are difficult to recycle only if chemical methods are used, the flax fiber reinforced epoxy serves as the first step for recyclable composites efforts. The epoxy-hardener ratio was 4:1 by weight, and the viscosity and glass transition temperature of the resin system were 450 MPa·s and 140 °C, according to the supplier's specifications. The fabrication process should be finished within 120 min outside the heating oven. Otherwise, the resin would cure spontaneously. Moreover, a closed-cell rigid foam (Rohacell-51 WF) based on polymethacrylimide (PMI) was selected to fabricate the foam sandwich panel. The mechanical properties of PMI and PMI foam are presented in Table 1.

2.1.2. Fabrication of laminates and foam sandwich panels

Flax fiber-reinforced laminates and foam sandwich composite panels were fabricated using VARI process. The composite layup schemes are presented in Fig. 1b. First, after painting the mold release

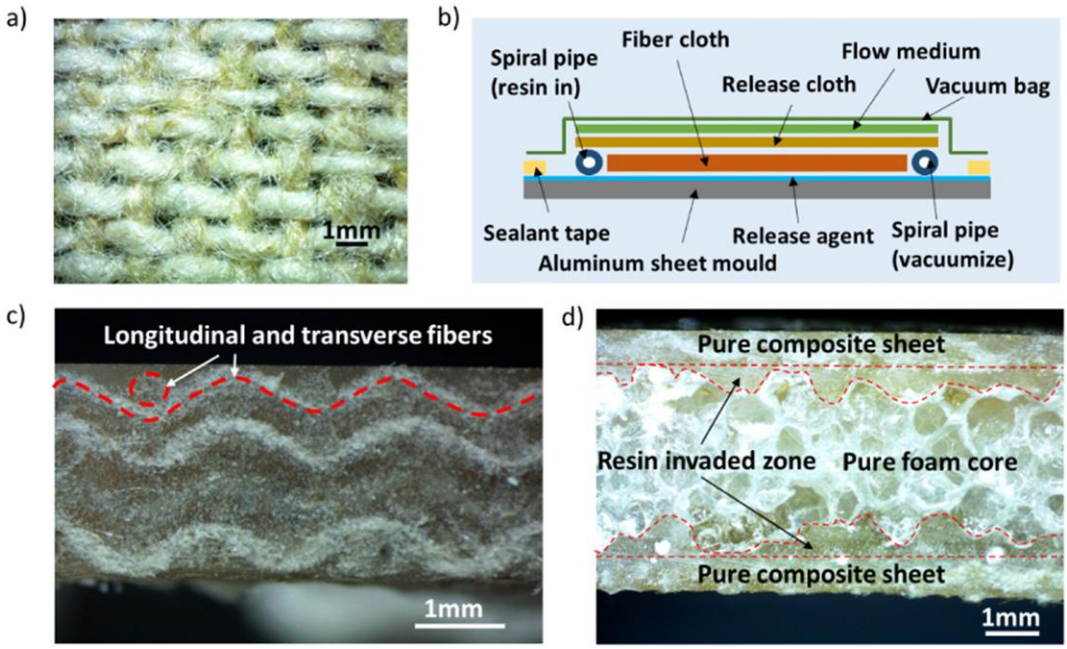

Fig. 1. a) Optical microscope image of flax fiber fabrics; b) the sketch of vacuum assisted resin infusion (VARI) process; c) the cross section of fabricated composite laminate and d) the cross section of foam sandwich panel with optical microscope.

agent, flax fabrics, demolding cloth, and flow medium were laid on an aluminum sheet. Specifically, four plies of flax fabrics were used for Type I and two plies for Types II and III (Table 2), while one ply of flax fabric was applied as face sheet for foam sandwich panels. Then, two spiral pipes were put aside the fabrics as illustrated, and the whole assembly was vacuum bagged (>0.09 MPa). Bagged samples were debulked for 20 min at room temperature to remove trapped air. Second, the epoxy resin solution was infused into the vacuum bagged assembly until the fabrics were fully saturated. Then, the whole assembly was transferred into an oven and cured at 80 °C for 2 h and 120 °C for 3 h. The mechanical properties of flax fiber are stable under 180 °C, so the curing temperature suggested by the supplier would not affect the properties of flax fiber. Finally, the flax fiber-reinforced laminates and foam sandwich panels were obtained after demolding from the aluminum sheet. The cross sections of the obtained laminates and foam sandwich panels were observed using an optical microscope, and the images are shown in Fig. 1c and d. The longitudinal and transverse fibers could be clearly observed in the flax woven fiber-reinforced laminates. Meanwhile, for the foam sandwich panel, a resin invaded zone existed around the interfaces caused by low-viscosity epoxy resin that flowed into the open cells of foams during infusion. Thus, the interfacial properties could be guaranteed as verified in the following section.

2.1.3. Fabrication of lattice cores

Pyramidal lattice cores with additional horizontal trusses of variable length were designed to optimize the overall mechanical properties with enhanced shear performance. The length of the horizontal trusses was flexible, and the optimal length value could be specified by considering both compression and shear performance. The representative volume cells for the monolithic and hierarchical lattice structures and corresponding geometrical parameters are shown in Fig. 2.

Monolithic and hierarchical lattice cores were fabricated by interlocking process as previously described [19], and the details are indicated in Fig. 3. Strips were first cut off from the flax fiber- reinforced laminates or foam sandwich panel and then grooved in to form the redesigned pyramidal lattice structure. Four types of lattice structures, including those with composite trusses and foam sandwich trusses, were fabricated, and the geometric parameters are summarized in Table 2. Types I, II, and III represent monolithic lattice cores with pure composites trusses of different relative densities, and Type IV stands for those with foam sandwich trusses. All lattice cores were subsequently glued with two composite face sheets forming sandwich structures (Fig. 4a–d) for the subsequent compression testing.

2.1.4. Equivalent density

The equivalent density of the redesigned lattice cores can be expressed as follows:

$$\rho_{equ} = \frac{2b(l_1 + l_3)t\rho_f}{(l_1\ \cos\omega + l_2 + b/\ \sin\omega)^2(l_1\ \cos\omega + 2b)} \quad (1)$$

where ρ_{equ} is defined as the mass of lattice core divided by the whole volume.

For hierarchical lattice cores with foam sandwich trusses, i.e., Type IV, $t\rho_f$ could be substituted with $2t_f\rho_f + t_c\rho_c$, where t_f and ρ_f are the thickness and density of face sheet, respectively, and t_c and ρ_c are the corresponding values of the foam cores in the sandwich strut.

Table 1
Mechanical properties of PMI material and foam.

Materials	Density (kg/m^3)	Compressive modulus (MPa)	Compressive strength (MPa)
PMI	1200	5200	90
Foam	52	75	0.8

Table 2
Geometric parameters for the four types of lattice structures.

Type		l_1 (mm)	l_2 (mm)	l_3 (mm)	ω	b (mm)	t (mm)	
Monolithic	I	8.94	6.34	30.34	$\pi/4$	2	2.43	
	II	8.94	6.34	12	$\pi/4$	2	1.23	
	III	12.73	9.51	18	$\pi/4$	3	1.23	
Hierarchical	IV	12.73	9.51	18	$\pi/4$	3	t_f	t_c
							0.5	4

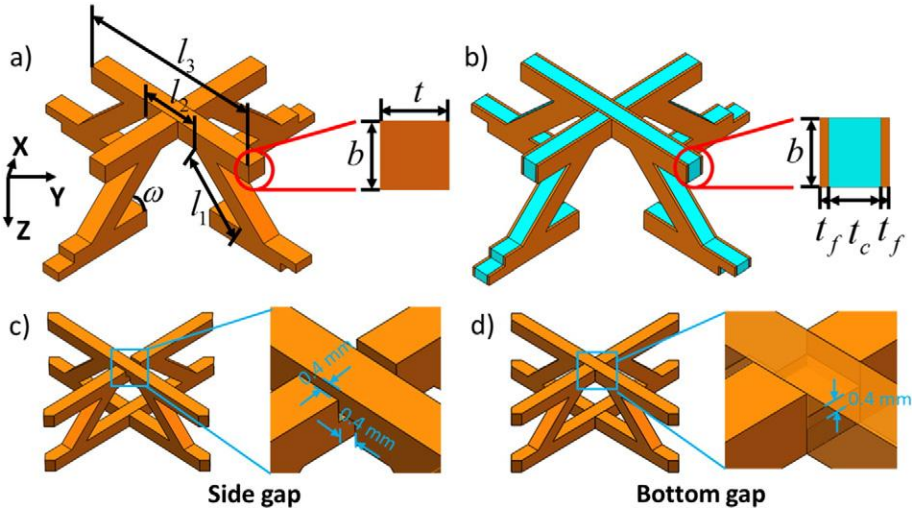

Fig. 2. The representative unit cells (RUC) for the redesigned pyramidal lattice structures with a) pure composite trusses; b) foam sandwich trusses with geometrical parameter illustrations. Defect type and size illustrations in the RUC FEA model: c) side gaps and d) bottom gap.

2.2. Testing

Through-thickness compression tests for the pyramidal lattice cores were performed on a hydraulic servo testing machine (MTS 810) at a displacement rate of 0.5 mm/min following ASTM C365/C365M [24]. Samples with 3 × 3 unit cells were prepared, and at least two repeated tests for each type of structure were performed to ensure the repeatability. The compression force was read from the load cell, while the compression displacement was measured using a laser extensometer.

The compression behavior of the obtained lattice structure was further examined by testing the struts in the same machine at the same compression velocity to obtain the compressive properties of constitutive materials. Each single strut was cut directly from the strips and clamped with two nuts on both ends to ensure verticality during testing.

3. Simulation

Defects probably occurred during fabrication at the contacting area (slots) between each two strips during the insertion at the nodes, including the side and bottom gaps, as illustrated in Fig. 2c and d. Numerical simulation was performed to investigate the sensitivity of defects on the compressive properties of lattice cores using ABAQUS/Explicit finite element program. Out-of-plane compression performance of representative unit cells with and without these two kinds of defects was simulated. During simulation, the unit cell was modeled (using SOLID element C3D8R following ABAQUS notation), and elements around the insertion zone were removed to simulate the gaps. The mesh size was set to 0.2 mm, and the gap was determined to be approximately 0.4 mm. Vertical displacement was applied on the top plate, while the bottom rigid plate was fully clamped, and periodic boundary conditions were applied on the free sides of the unit cell. Lattice cores with three different lengths l_2 (2, 4.8 and 6.34 mm) were simulated. The material property of the lattice element was determined from the experiments, and an elastoplastic model with ductile damage strain was employed.

4. Analysis

4.1. Properties of foam

Gibson and Ashby [25] showed that the mechanical properties of a closed-cell foam are related to its relative density $\overline{\rho}_c = \rho_c/\rho_s$. The Young's modulus E_c, shearing modulus G_c, and shearing strength τ_c of foams can be described as follows:

$$E_c/E_s = \phi^2\overline{\rho}_c^2 + (1-\phi)\overline{\rho}_c \tag{2}$$

$$G_c \approx \frac{3}{8}E_c \tag{3}$$

$$\tau_c/\sigma_s = 0.2\phi^{3/2}\overline{\rho}_c^{3/2} + (1-\phi)\overline{\rho}_c \tag{4}$$

In the present study, parameters could be obtained from Table 1, i.e., $E_s = 5200$ MPa, $\sigma_s = 90$ MPa, $\rho_s = 1200$ kg/m^3, $E_c = 75$ MPa, and $\rho_c = 52$ kg/m^3. The shearing modulus and strength of foam are

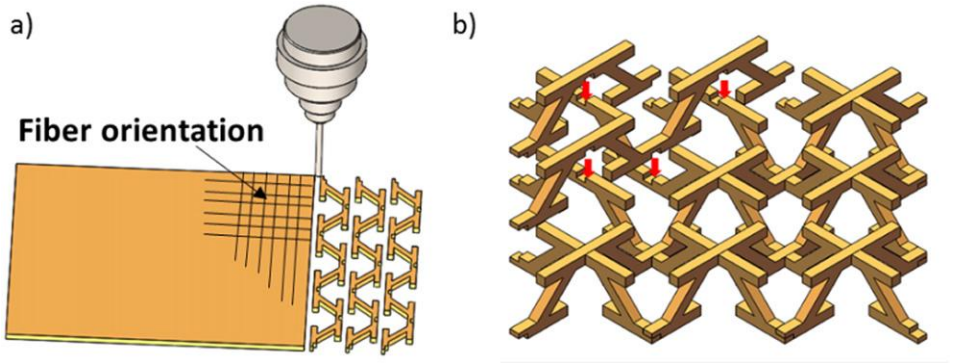

Fig. 3. The fabrication flow chart of the redesigned pyramidal lattice structures: a) truss strips cutting from composite/sandwich sheet; b) the assembled pyramidal lattice structure.

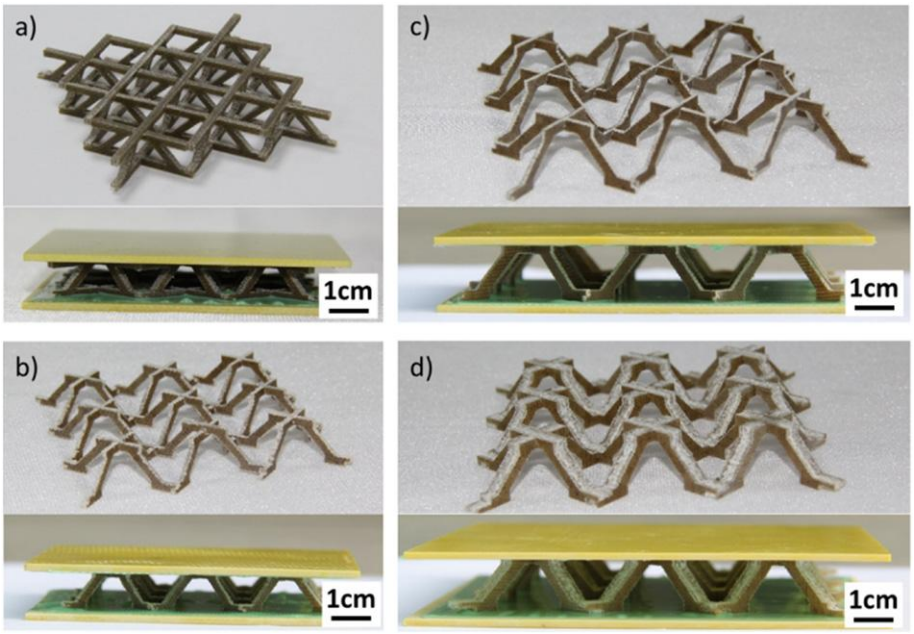

Fig. 4. Sandwich structures for compression testing: a), b), c) monolithic lattice structures with pure composite trusses with different geometric parameters; d) hierarchical lattice structure with foam sandwich trusses.

$G_c = 24$ MPa and $\tau_c = 0.8$ MPa, respectively, and the volume ratio ϕ is assumed to be 0.6.

4.2. Homogenized constitutive model for redesigned pyramidal lattice cores

The pyramidal lattice cores have in-plane (X-Y) symmetry and can be termed as orthotropic which has nine independent elastic constants. The linear elastic strain tensor ε_i and stress tensor σ_j relationship (with Cartesian indices) can be expressed as follows:

$$\begin{Bmatrix} \varepsilon_{XX} \\ \varepsilon_{YY} \\ \varepsilon_{ZZ} \\ \gamma_{YZ} \\ \gamma_{XZ} \\ \gamma_{XY} \end{Bmatrix} = \begin{bmatrix} S_{XXXX} & S_{XXYY} & S_{XXZZ} & 0 & 0 & 0 \\ S_{YYXX} & S_{YYYY} & S_{YYZZ} & 0 & 0 & 0 \\ S_{ZZXX} & S_{ZZYY} & S_{ZZZZ} & 0 & 0 & 0 \\ 0 & 0 & 0 & S_{YZYZ} & 0 & 0 \\ 0 & 0 & 0 & 0 & S_{XZXZ} & 0 \\ 0 & 0 & 0 & 0 & 0 & S_{XYXY} \end{bmatrix} \begin{Bmatrix} \sigma_{XX} \\ \sigma_{YY} \\ \sigma_{ZZ} \\ \tau_{YZ} \\ \tau_{XZ} \\ \tau_{XY} \end{Bmatrix} \quad (5)$$

where the elastic compliance matrix S_{ij} can be given with engineering elastic constants according to the mechanics of composite materials [26], as follows:

$$S = \begin{bmatrix} \frac{1}{E_X} & \frac{-\upsilon_{YX}}{E_Y} & \frac{-\upsilon_{ZX}}{E_Z} & 0 & 0 & 0 \\ \frac{-\upsilon_{XY}}{E_X} & \frac{1}{E_Y} & \frac{-\upsilon_{ZY}}{E_Z} & 0 & 0 & 0 \\ \frac{-\upsilon_{XZ}}{E_X} & \frac{-\upsilon_{YZ}}{E_Y} & \frac{1}{E_Z} & 0 & 0 & 0 \\ 0 & 0 & 0 & \frac{1}{G_{XY}} & 0 & 0 \\ 0 & 0 & 0 & 0 & \frac{1}{G_{YZ}} & 0 \\ 0 & 0 & 0 & 0 & 0 & \frac{1}{G_{ZX}} \end{bmatrix} \quad (6)$$

The effective elastic constant in the elastic compliance matrix are deduced in Appendix. As shown in the Appendix, the equivalent in-plane modulus, $E_X = E_Y$, and the effective Poisson's ratios, υ_{XZ}, υ_{ZX}, υ_{YZ}, and υ_{ZY}, are considered to be approximately zero, while υ_{YX} is calculated to be approximately 1 when $\varphi = \omega = \pi/4$. Contrary to the published work [27], the bending effect of lattice trusses was also considered in the current study.

4.3. Collapse mechanism map

Compressive strength of the redesigned pyramidal lattice truss cores was analyzed similar to the deduction in a previous work [19] and will not be repeated here. Euler buckling (EB) and strut crushing (SC) of lattice trusses are two possible failure modes for monolithic lattice cores. By contrast, five possible failure modes, namely, face sheet crushing (FC), EB, shear buckling (SB), face sheet wrinkle (FW), and foam core shear failure (CSF), exist for hierarchical lattice cores with foam sandwich trusses [20]. The horizontal trusses rarely affected the compression behavior of lattice cores in the present study.

Subsequently, collapse mechanism maps, which are useful for engineers to select a structural geometry with predictable strength, were constructed for monolithic and hierarchical pyramidal lattice cores under compression. For monolithic lattice structures (Types I to III), the map was constructed as a function of b/l_1(0–0.4) or t/l_1(0–0.4) and σ_f/E_f(0–0.1) (Fig. 5a). Similarly, for hierarchical lattice structures (Type IV), the collapse mechanism map was constructed by altering the relative density of foam core $\overline{\rho}_c$(0–0.2) and the ratio t_c/l_1(0–0.5) with the same $t_f/l_1 = 0.071$ and inclination angle of $\omega = 45^\circ$. Four different failure modes, namely, SB, FW, FC, and EB, were observed in the map (Fig. 5b). CSF did not appear in the map. All experimental results were marked in the corresponding map, and the experimental results showed great agreement with theoretical predicted results.

5. Results and discussion

5.1. Compressive properties of constitutive materials

Compression tests were performed on composite struts which provided the mechanical properties of flax-fiber reinforced composites. The stress-strain curves with good consistency are shown in Fig. 6. For a typical stress-strain curve, an initial linear elastic stage appeared, followed by a yield stage and a strengthening stage. The slope of the linear stage was the compressive modulus, while the stress corresponding to the strain value read from the intersection point of the tangents to the linear stage and the strengthening stage served as the yield strength. The calculated compressive modulus and strength were 1.464 GPa and

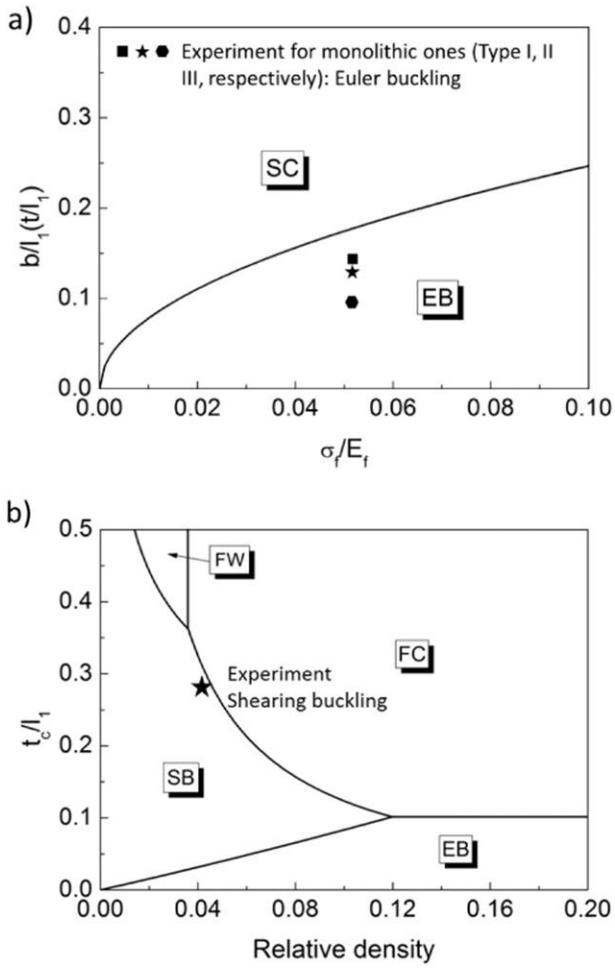

Fig. 5. Collapse mechanism map of a) monolithic lattice cores with pure composite trusses; b) hierarchical lattice cores with foam sandwich trusses.

74.092 MPa, respectively. The difference caused by the fabrication process was not significant such that the composite sheets with different thickness were regarded to share the same mechanical properties.

5.2. Compressive properties of lattice cores

All four types of lattice structures were tested under through-thickness compression, and the stress-strain curves were compared

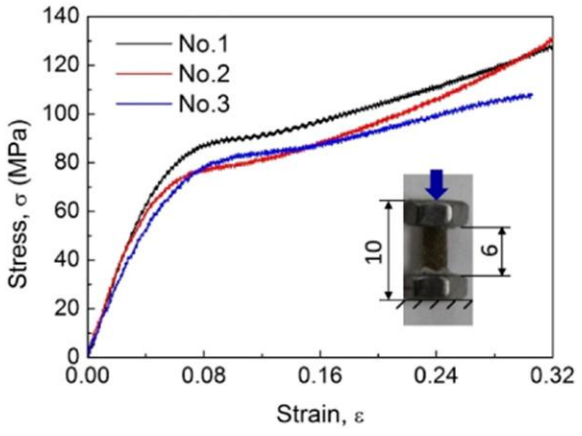

Fig. 6. Compressive stress-strain curves derived from compression tests of single strut cut from the flax fiber reinforced composite plates.

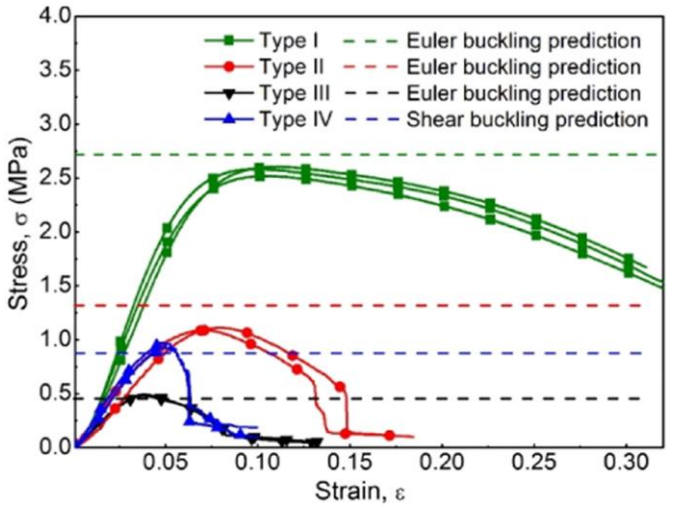

Fig. 7. Compressive stress-strain curves of four different types of lattice structures comparing with theoretical prediction.

and are shown in Fig. 7. The green, red, black, and blue lines represent Types I, II, III, and IV lattice structures, respectively. All curves have initially elastic linear increasing stages from which the nominal compressive modulus of structure was determined. A relatively long strain softening stage followed by the peak point appeared in the monolithic lattice structures, while the stress decreased more sharply for hierarchical lattice structures (Type IV). Theoretical strength prediction values for all four types of lattice structures are shown in Fig. 7. All theoretical predictions may satisfactorily predict the compressive strength with deviations of 6.25%, 15.45%, −8.16%, and −8.42% for Types I, II, III, and IV,

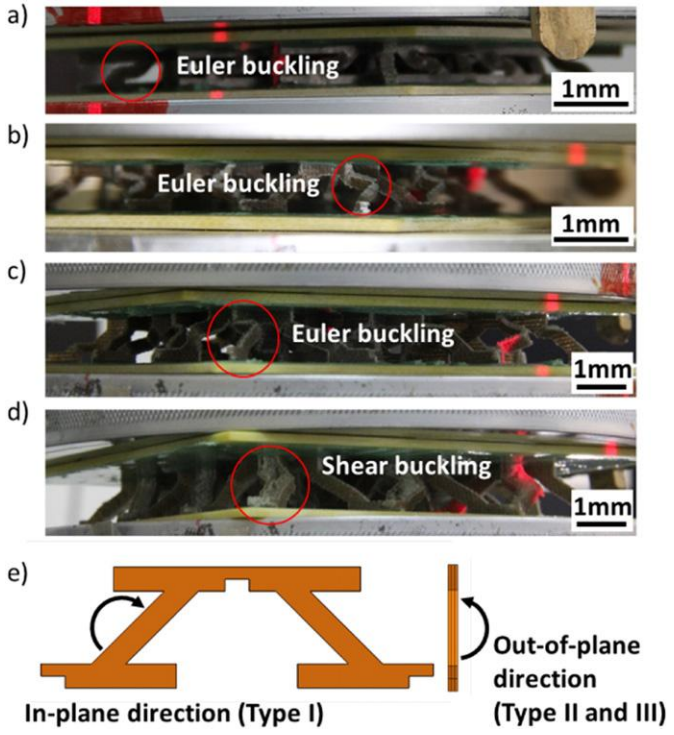

Fig. 8. Failure modes of different composite lattice structures: a–c) Euler buckling for monolithic ones (Type I–III) and d) shear buckling for hierarchical one (Type IV); and e) illustration about different buckling modes for monolithic lattice structures: bucking along in-plane direction for Type I structure and along out-of-plane direction for Type II and III structures.

Table 3
Through-thickness compressive properties and equivalent density.

Type	ρ_{equ} (g/cm^3)	Nominal strength (MPa)	Nominal stiffness (MPa)	Specific strength (MPa·m^3/kg)	Specific stiffness (MPa·m^3/kg)
I	0.182	2.56 ± 0.03	42.76 ± 1.64	1.41×10^{-2}	0.235
II	0.057	1.1 ± 0.01	21.58 ± 0.98	1.93×10^{-2}	0.379
III	0.035	0.49 ± 0.005	16.29 ± 0.43	1.40×10^{-2}	0.465
IV	0.033	0.95 ± 0.02	23.45 ± 0.49	2.88×10^{-2}	0.711

respectively. The differences between experimental and predictive results could be attributed to the possible defects generated in the composite sheets during fabrication, and the assumption that composite sheets with different thicknesses share the same moduli and strengths. Fig. 8a–d show that different kinds of lattice structures exhibit various failure modes. For Type I, the struts fail by EB which may be attributed to the low moment of inertia caused by the slender shape and relatively poor compressive stiffness of the parent material, i.e., flax fiber-reinforced composite sheet compared with carbon fiber counterparts. Types II and III show the same failure modes, but the struts buckled in different directions compared with Type I. The difference is illustrated in Fig. 8e, in which the moment vector causing EB in Type I was along the in-plane direction of the composite strut sheet but along the out-of-plane direction in Types II and III. For Type IV, the governing failure mode of the lattice truss core sandwich structures is SB. Compared with a previous study [20], the structure in the current study did not fail by FW, which should be attributed to the enhanced interfacial property by resin infusion process.

The compressive properties are summarized in Table 3 along with the specific stiffness and strength. For monolithic lattice cores, the nominal compressive strength and stiffness varied linearly with the equivalent density (Type I to III). The corresponding values for hierarchical lattice cores were greater than those of the monolithic ones (Type III) with comparable relative densities of 94% and 44%. The utilization of foam increased the compressive strength and stiffness with a relatively low equivalent density. The four lattice structures were found to vary distinctly after dividing the strength and modulus by the equivalent density. Type II reached the highest specific strength among monolithic structures, and this parameter was determined directly by the corresponding radius of inertia. Type IV showed the highest specific nominal stiffness and strength values, which were approximately 1.5× and 2× those for monolithic lattice cores.

Table 4
Measured compressive strength compared with other cellular core materials.

Cellular material	ρ_{equ} (kg/m^3)	Compressive strength (MPa)	Specific strength (MPa·m^3/kg)
Lattice cores (Type IV)	33	0.95	0.0288
CFRP tetrahedral lattice [28]	53.82	4.6	0.0855
Al tetrahedral [29]	99.2	6.1	0.0615
Steel pyramidal lattice [30]	210.6	4.32	0.0205
CFPR pyramidal lattice [9]	100	9	0.09
5052Al honeycombs [13]	33	0.91	0.0276
Nomex honeycombs [31]	32	0.85	0.0266
Al foam-filled corrugated cores [32]	1106	25.6	0.0231
Al foam [33]	224	1.55	0.0069

5.3. Defect sensitivity

The compressive responses of representative unit cells with and without defects are shown in Fig. 9. Fig. 9a and b show the compressive deformation mode and stress-strain curves of Type I lattice cores ($t = 2$mm) by simulation compared with those of experimental results to validate the FEA model. The deformation mode of EB calculated by simulation was the same as that obtained experimentally. The stiffness

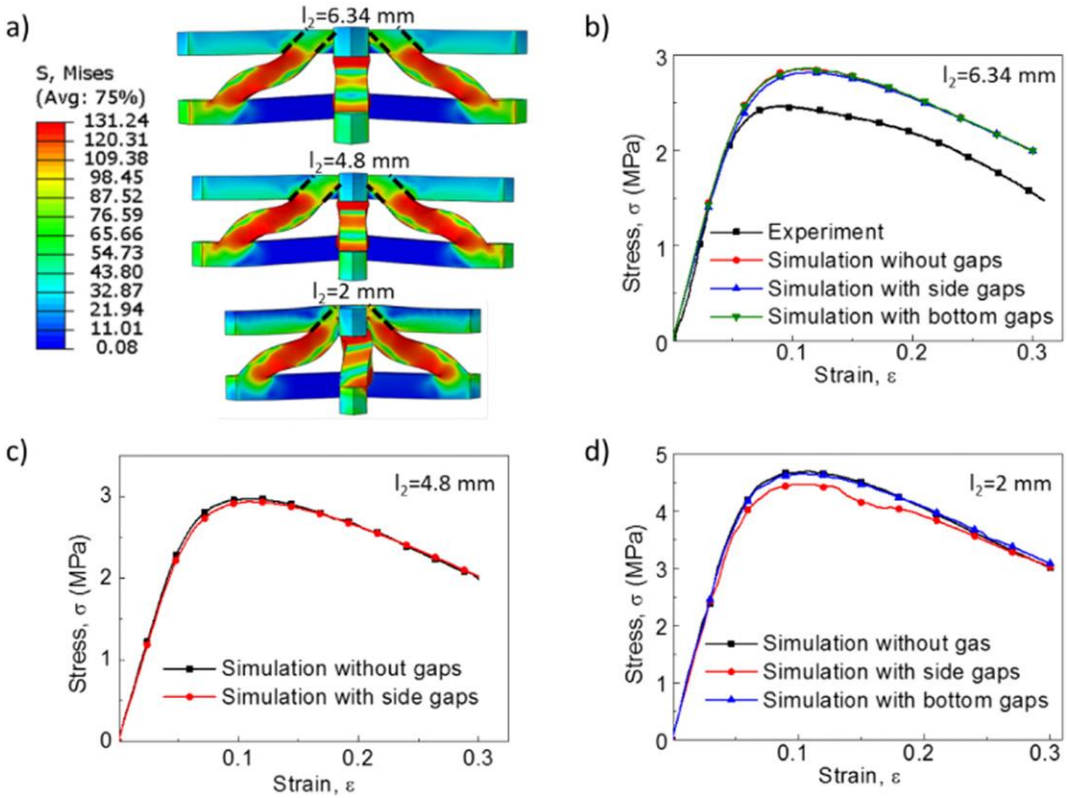

Fig. 9. a) Deformation mode and stress distribution of Type I lattice cores with variable l_2 by simulation. When $l_2 = 6.34$mm and 4.8 mm, the stress distribution along the inclined struts will not be interfered by side gaps at the slots, while will be affected as $l_2 = 2$mm. b–d) The effective stress-strain curves of representative unit cells with and without defects with different l_2. The effects about bottom gaps have rarely no effect on the compressive properties, while those about side gaps depends on l_2.

value was also the same while the deviation of strength value was approximately 10%, which is acceptable.

The compressive stress-strain curves of the representative unit cells of Type I, including the side and bottom gaps, were simulated, and the results are shown in Fig. 9b. No evident influence was observed when either side gap or bottom gap was introduced. Subsequently, lattice core with variable length l_2 was simulated as shown in Fig. 9c ($l_2 =$ 4.8mm) and 9d ($l_2 = 2$mm). The effects of the bottom gaps showed relatively no effect on the compressive properties, while those of side gaps were dependent on l_2, and lattice cores with short l_2 was weakened by these defects. A transition l_2 may exist, because the stress distribution at the truss ends will not be interfered by the slots if l_2 (and thus length of horizontal truss l_3, $l_3 > l_2$) is large enough.

An approximate transition value of length l_2 could be deduced by assuming that the stress was distributed within the outline of the inclined strut and would have little effect to the surrounding area, as follows:

$$l_2^{tran} = (b/2\ \tan\omega) \times 2 + t + w_{gap} = b/\ \tan\omega + t + w_{gap} \tag{7}$$

where the $w_{gap} = t_p - t$ is the length of the side gap. Note that t_p is the width of slot after polishing (2.8 mm). Thus, the transition length l_2 is approximately 4.8 mm, which was also validated by simulation.

5.4. Comparison with other materials

The hierarchical structure had a similar configuration with the hierarchical carbon fiber lattice structure in [19]. However, the failure mode of the latter was FW, which should be attributed to the poor interfacial property such that the former one was more efficient. Comparison between the hierarchical lattice structure (Type IV) and other typical cellular materials are summarized in Table 4. The specific strength of the hierarchical structures was superior to those of steel lattice and Al foam-filled corrugated core and competitive with Nomex honeycombs. The specific compressive strength values versus effective density and cost of these cellular materials are also plotted in Fig. 10. The cost of cellular materials consists of raw material cost and manufacturing cost. However, the manufacturing cost is usually complex to calculate and thus in the present study only raw material cost is included to evaluate that of cellular materials. A roughly objective function expressing cost per volume C_V of cellular materials was assumed to be the cost of raw materials. Thus, Eq. (8) was established, as follows:

$$C_V = c_{kg} \times \rho_{equ} \tag{8}$$

The flax fiber-reinforced lattice cores in the present study occupy the low-cost area in the chart in Fig. 10b, although its specific compressive strength is inferior to that of CFRP lattice core. The low cost and recyclability with natural fiber reinforcement make the fabricated materials promising in automotive industries.

6. Concluding remarks

Natural fibers facilitate the development of environment-friendly lightweight materials and structures. Flax fiber-reinforced composite lattice materials were developed in the present study. Monolithic and hierarchical composite pyramidal lattice materials were designed with additional horizontal beams of variable length for optimized overall mechanical properties. The flax fiber-reinforced composite lattice cores with pure composites and foam sandwich struts were fabricated via a low-cost VARI and slot assembly method. An orthotropic constitutive model of the redesigned pyramidal lattice cores was proposed. All components of the elastic compliance matrix were expressed with lattice geometry and elastic constants of parent materials.

Out-of-plane compressive performance of the monolithic and hierarchical lattice core sandwich structures with different geometries was then examined. For the monolithic lattice cores, the struts tended to fail by EB along the direction with lower moment of inertia, while the governing failure mode of the hierarchical cores was truss SB. The specific nominal stiffness and strength values of the hierarchical construction were approximately 1.5× and 2× those for their monolithic counterparts. Moreover, theoretical models were established to predict the compressive strength, and collapse mechanism maps for flax fiber-reinforced monolithic and hierarchical lattice cores were established. The prediction models could well predict the compressive strength with deviations of 6.25%, 15.45%, −8.16%, and −8.42% for Types I, II, III, and IV, respectively. Defect sensitivity of the redesigned lattice cores was studied by simulation of the representative unit cells in compression. Effects of side and bottom gaps were examined for monolithic lattice cores. The bottom gaps did not evidently affect the compressive properties, while the effects of side gaps were dependent on the length l_2 between two inclined struts. Lattice cores with relatively short l_2 (and length of horizontal truss l_3, $l_3 > l_2$) were weakened by side defects, and a reasonable transition value of l_2 was also deduced. This value will guide the optimal design of the length of horizontal trusses for the lattice geometry.

The flax fiber-reinforced composite lattice structures in the present study could be superior to several metallic lattice structures, foam filled corrugated materials, and competitive with Nomex honeycombs. Moreover, the flax fiber-reinforced lattice structures can fill low-cost gaps in the property-cost chart, although their mechanical properties are not comparable with carbon fiber-reinforced counterparts. Given their low-cost and conceivable recyclability, natural fiber-reinforced lattice materials are promising lightweight candidates with excellent mechanical properties and strong

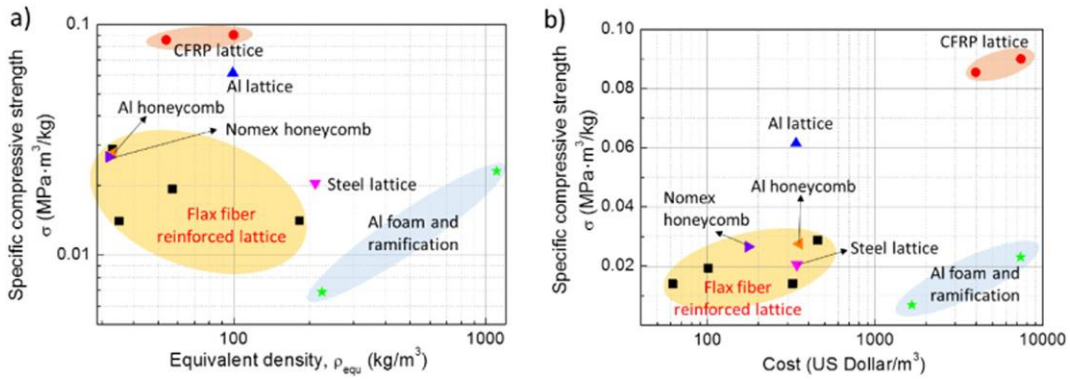

Fig. 10. Specific compressive strength of different cellular materials listed in Table 4 vs. (a) equivalent density; (b) structure cost per volume.

designability. The results may provide insight on the feasibility of applying natural fiber lattice materials in the automotive industry to improve vehicle efficiency and emission. Specific application of these materials will be investigated further.

Acknowledgements

This work is financially supported by the National Natural Science Foundation of China under grant No. 11402012, Young Elite Scientist Sponsorship Program by CAST, Opening fund of State Key Laboratory for Strength and Vibration of Mechanical Structures, Xi'an Jiaotong University (SV2015-KF-07, SV2016-KF-20), Opening fund of State Key Laboratory for Automotive Safety and Energy, Tsinghua University (Grant No. KF16142), and Beijing Municipal Science & Technology Commission (Grant No.Z161100001416006).

Appendix A. Engineering elastic constants prediction

A.1. Compressive stiffness

As shown in Fig. A1, taking stretching and all bending (shearing deformation is involved for Type IV) in consideration, the axial and shear force, F_a and F_s, in the strut can be written as:

$$F_a = A\frac{\delta\ \sin\omega}{l_1}\ \text{and}\ F_s = \frac{\delta\ \cos\omega}{\frac{{l_1}^3}{12D}+\frac{l_1}{S}} \qquad (A-1)$$

where $A = E_f tb$ ($A = 2E_f t_f b$ for lattice structure with foam sandwich trusses), $D = \frac{1}{12}E_f tb^3$ or $D = \frac{1}{12}E_f bt^3$ ($D = \frac{1}{2}E_f bt_f t_c^2$ for lattice structure with foam sandwich trusses) and $S = G_c bt_c$ (only for lattice structure with foam sandwich trusses).

The total force in through-thickness direction (Z direction) of a single strut can be expressed as:

$$F' = \frac{F}{4} = F_a\ \sin\omega + F_s\ \cos\omega = \delta\left(\frac{\sin^2\omega}{\frac{l_1}{A}}+\frac{\cos^2\omega}{\frac{{l_1}^3}{12D}+\frac{l_1}{S}}\right) \qquad (A-2)$$

Then the equivalent out-of-plane compression stiffness is:

$$E_Z = \frac{F}{A_s\varepsilon} = \frac{2(l_1\ \sin\omega + 2b)}{(l_1\ \cos\omega + l_2 + b/\ \sin\omega)^2}\left(\frac{\sin^2\omega}{\frac{l_1}{A}}+\frac{\cos^2\omega}{\frac{{l_1}^3}{12D}+\frac{l_1}{S}}\right) \qquad (A-3)$$

where $\varepsilon = \delta/(l_1\sin\omega + 2b)$ is the nominal strain. Note that term l_1/S is only valid for the hierarchical lattice structures with foam sandwich trusses.

As shown in Fig. A2, when the RUC is compressed along the in-plane direction, the corresponding compressive stiffness can be given by analyzing the symmetric semi RUC in the similar way shown above as:

$$E_X = E_Y = \frac{F'/\ \cos\varphi}{A_s 2\varepsilon'/\ \cos\varphi} = \frac{\sqrt{2}}{(l_1\ \sin\omega + 2b)}\left(\frac{\cos^2\omega}{\frac{l_1}{A}}+\frac{\sin^2\omega}{\frac{{l_1}^3}{12D}+\frac{l_1}{S}}\right) \qquad (A-4)$$

A.2. Shear stiffness

Like the theoretical analysis of in-plane compressive stiffness in Section A.1, a semi RUC is applied with force F, shown in Fig. A2. The axial and shear force of a single strut can be written similarly as Eq. (A-1) and then the total force of one strut also has the same form with

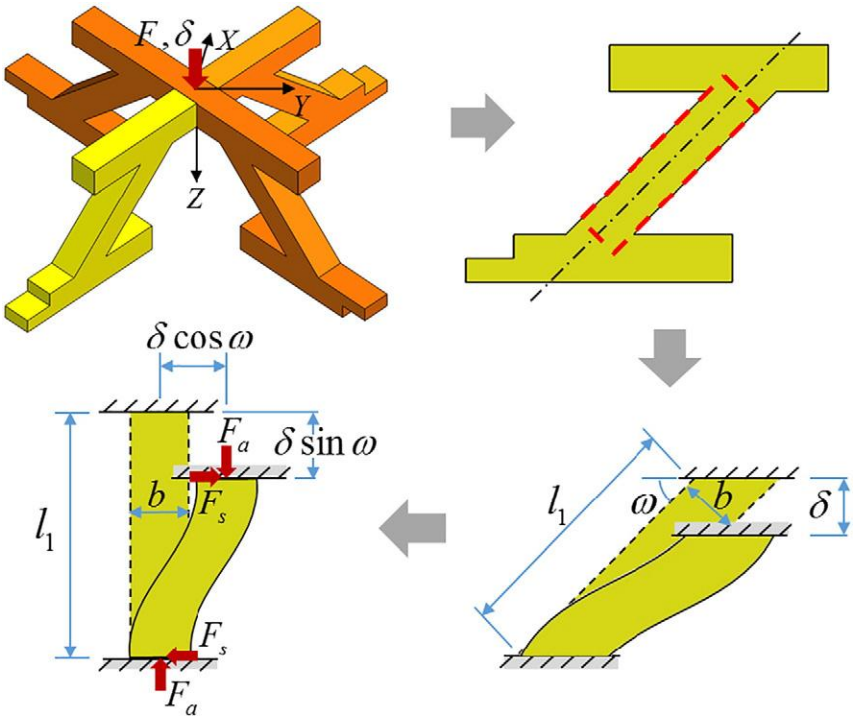

Fig. A1. Sketch of the deformation of a single strut under through-thickness compression and the free body diagram showing combined axial and shear forces.

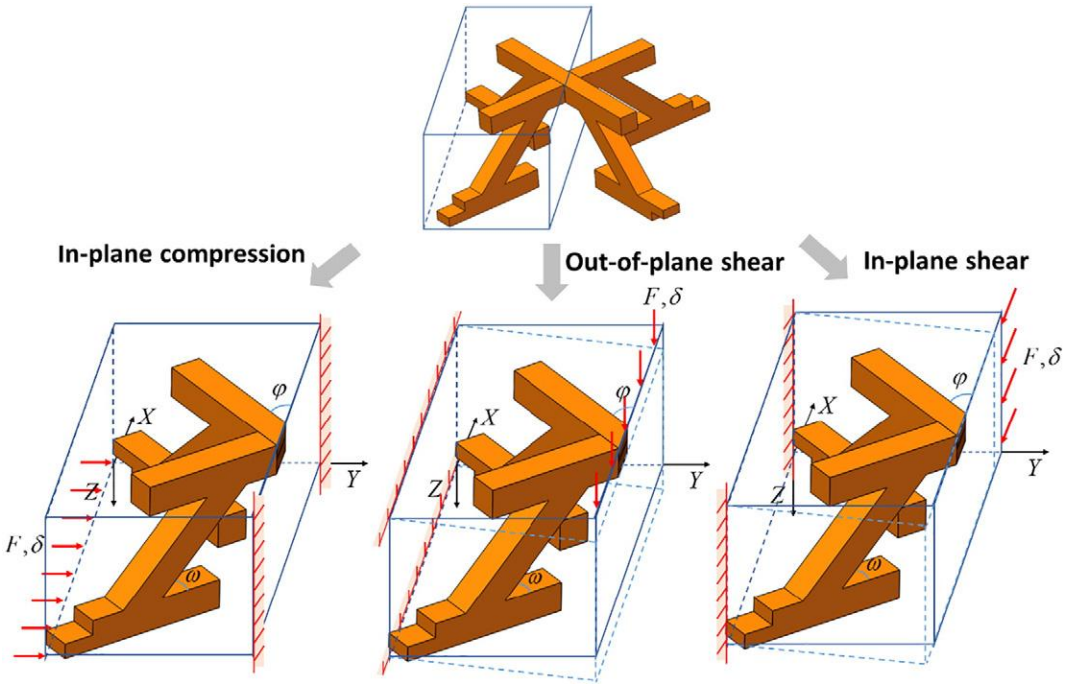

Fig. A2. Sketch of force and deformation of semi unit cells under in-plane compression, out-of-plane shear and in-plane shear, respectively.

Eq. (A-2). Thus, the equivalent out-of-plane shear stiffness is:

$$G_{XZ} = \frac{2}{(l_1 \sin\omega + 2b)}\left(\frac{\sin^2\omega}{\frac{l_1}{A}} + \frac{\cos^2\omega}{\frac{{l_1}^3}{12D} + \frac{l_1}{S}}\right) \quad (A-5)$$

Similarly, when the semi unit cell is applied with an in-plane force F, also as shown in Fig. A2, the equivalent in-plane shear stiffness can be given as:

$$G_{XY} = \frac{1}{\cos\varphi(l_1 \sin\omega + 2b)}\left(\frac{\cos^2\omega}{\frac{l_1}{A}} + \frac{\sin^2\omega}{\frac{{l_1}^3}{12D} + \frac{l_1}{S}}\right) \quad (A-6)$$

A.3. Poisson's ratio

As shown in Fig. A3, when the structure is compressed along the in-plane direction, the struts would deform both in X and Y direction, which produces the Poisson's ratio, υ_{YX}. Assuming that the in-plane compression is carried out by applying concentrated force on end of each strut, then a single strut is analyzed due to the symmetry of the unit cell. According to Eq. (A-2) and ignoring the shearing effect, the deformation of the unit cell in X and Y direction can be written out respectively:

$$\delta_x = \frac{F\sin\varphi\cos\varphi {l_1}^3}{3E_f I} - \frac{F\cos\varphi\sin\varphi l_1}{E_f bt\left(\cos^2\omega + \frac{b^2}{{l_1}^2}\sin^2\omega\right)} \quad (A-7)$$

$$\delta_y = \frac{F\sin^2\varphi {l_1}^3}{3E_f I} + \frac{F\cos^2\varphi l_1}{E_f bt\left(\cos^2\omega + \frac{b^2}{{l_1}^2}\sin^2\omega\right)} \quad (A-8)$$

Thus, the Poisson's ratio, υ_{YX} can be written as:

$$\upsilon_{YX} = -\frac{4\sin\varphi\cos\varphi\left({l_1}^2\cos^2\omega + b^2\sin^2\omega\right) - t^2\sin\varphi\cos\varphi}{4\sin^2\varphi\left({l_1}^2\cos^2\omega + b^2\sin^2\omega\right) + t^2\cos^2\varphi} \quad (A-9)$$

when $\varphi = \omega = \pi/4$, υ_{YX} can be expressed as $\upsilon_{YX} = -[2({l_1}^2/t^2 + b^2/t^2) - 1]/[2({l_1}^2/t^2 + b^2/t^2) + 1]$, approximately equal to 1 when $l_1/t \geq 4$.

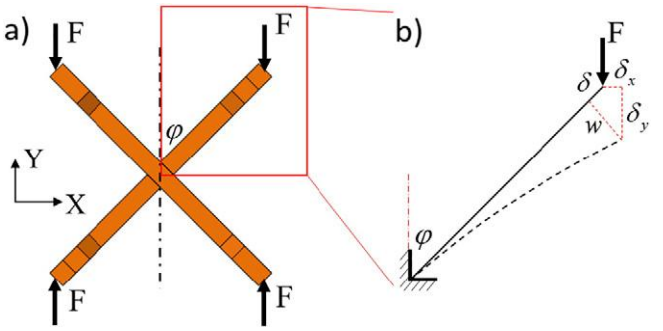

Fig. A3. Schematic illustration about the deduction of Poisson's ratio, υ_{YX}: a) four concentrated forces are assumed to impose at strut ends; b) deformation of a single strut in X-Y plane after compressing.

References

[1] C. Schilde, H. Nolte, C. Arlt, A. Kwade, Effect of fluid–particle-interactions on dispersing nano-particles in epoxy resins using stirred-media-mills and three-roll-mills, Compos. Sci. Technol. 70 (2010) 657–663.
[2] J.R. Duflou, Y. Deng, K.V. Acker, W. Dewulf, Do fiber-reinforced polymer composites provide environmentally benign alternatives? A life-cycle-assessment-based study, MRS Bull. 37 (2012) 374–382.
[3] K.C. Cheung, N. Gershenfeld, Reversibly assembled cellular composite materials, Science 341 (2013) 1219–1221.
[4] K. Lee, K. Ahn, J. Yoo, A novel P-norm correction method for lightweight topology optimization under maximum stress constraints, Comput. Struct. 171 (2016) 18–30.

[5] M.F. Ashby, The CES EduPack Database of Natural and Man-made Materials, 2008.
[6] G. Lu, T. Yu, Energy Absorption of Structures and Materials, Woodhead, Cambridge, 2003.
[7] N.A. Fleck, M.F. Ashby, Micro-architectured materials: past, present and future, Proc. R. Soc. A 466 (2010) 2495–2516.
[8] T. Li, L. Wang, Bending behavior of sandwich composite structures with tunable 3D-printed core materials, Compos. Struct. 175 (2017) 46–57.
[9] K. Finnegan, G. Kooistra, H.N.G. Wadley, V.S. Deshpande, The compressive response of carbon fiber composite pyramidal truss sandwich cores, Int. J. Mater. Res. 98 (2007) 1264–1272.
[10] K.P. Dharmasena, H.N.G. Wadley, K. Williams, Z. Xue, J.W. Hutchinson, Response of metallic pyramidal lattice core sandwich panels to high intensity impulsive loading in air, Int. J. Impact Eng. 38 (2011) 275–289.
[11] G.J. Mcshane, V.S. Deshpande, N.A. Fleck, Underwater blast response of free-standing sandwich plates with metallic lattice cores, Int. J. Impact Eng. 37 (2010) 1138–1149.
[12] L. Xiao, W. Song, C. Wang, H. Tang, N. Liu, J. Wang, Yield behavior of open-cell rhombic dodecahedron Ti-6Al-4V lattice at elevated temperatures, Int. J. Mech. Sci. 115–116 (2016) 310–317.
[13] B. Russell, V. Deshpande, H. Wadley, Quasistatic deformation and failure modes of composite square honeycombs, J. Mech. Mater. Struct. 3 (2008) 1315–1340.
[14] D. Liang, H. Wadley, Shear response of carbon fiber composite octet-truss lattice structures, Compos. Part A 81 (2016) 182–192.
[15] Y. Liu, T.A. Schaedler, A.J. Jacobsen, X. Chen, Quasi-static energy absorption of hollow microlattice structures, Compos. Part B 67 (2014) 39–49.
[16] Y. Liu, T.A. Schaedler, X. Chen, Dynamic energy absorption characteristics of hollow microlattice structures, Mech. Mater. 77 (2014) 1–13.
[17] S. Yin, L. Wu, L. Ma, S. Nutt, Pyramidal lattice sandwich structures with hollow composite trusses, Compos. Struct. 93 (2011) 3104–3111.
[18] S. Yin, L. Wu, L. Ma, S. Nutt, Hybrid truss concepts for carbon fiber composite pyramidal lattice structures, Compos. Part B 43 (2012) 1749–1755.
[19] S. Yin, L. Wu, S. Nutt, Stretch–bend-hybrid hierarchical composite pyramidal lattice cores, Compos. Struct. 98 (2013) 153–159.
[20] S. Yin, J. Li, B. Liu, K. Meng, H. Yong, S.R. Nutt, J. Xu, Honeytubes: hollow lattice truss reinforced honeycombs for crushing protection, Compos. Struct. 160 (2016).
[21] S. Yin, L. Wu, S.R. Nutt, Compressive efficiency of stretch–stretch-hybrid hierarchical composite lattice cores, Mater. Des. 56 (2014) 731–739.
[22] M. Li, L. Wu, L. Ma, B. Wang, Z. Guan, Mechanical Response of All-composite Pyramidal Lattice Truss core Sandwich Structures, J. Mater. Sci. Technol. 27 (2011) 570–576.
[23] Z. Mahboob, I.E. Sawi, R. Zdero, Z. Fawaz, H. Bougherara, Tensile and compressive damaged response in Flax fibre reinforced epoxy composites, Compos. Part A 92 (2017) 118–133.
[24] C.C.M.A.D. Committee, Standard Test Method for Flatwise Compressive Properties of Sandwich Cores, 2011.
[25] L.J. Gibson, M.F. Ashby, Cellular Solids: Structure and Properties, Cambridge University Press, Cambridge, 1997.
[26] A. Malkin, S. Kulichikhin, P. Astakhov, Y. Chernov, V. Kozhina, L. Golubenkova, Mechanics of Composite Materials, Wiley, 1979.
[27] L. Dong, V. Deshpande, H. Wadley, Mechanical response of Ti–6Al–4V octet-truss lattice structures, Int. J. Solids Struct. 60–61 (2015) 107–124.
[28] G. Zhang, L. Ma, B. Wang, L. Wu, Mechanical behaviour of CFRP sandwich structures with tetrahedral lattice truss cores, Compos. Part B 43 (2012) 471–476.
[29] G.W. Kooistra, V.S. Deshpande, H.N.G. Wadley, Compressive behavior of age hardenable tetrahedral lattice truss structures made from aluminium, Acta Mater. 52 (2004) 4229–4237.
[30] F.W. Zok, S.A. Waltner, Z. Wei, H.J. Rathbun, R.M. Mcmeeking, A.G. Evans, A protocol for characterizing the structural performance of metallic sandwich panels: application to pyramidal truss cores, Int. J. Solids Struct. 41 (2004) 6249–6271.
[31] X.Z. Wang, L.Z. Wu, S.X. Wang, Tensile and shear properties of aluminium foam, Mater. Technol. 24 (2013) 161–165.
[32] L.L. Yan, B. Yu, B. Han, C.Q. Chen, Q.C. Zhang, T.J. Lu, Compressive strength and energy absorption of sandwich panels with aluminum foam-filled corrugated cores, Compos. Sci. Technol. 86 (2013) 142–148.
[33] I. Jeon, T. Asahina, The effect of structural defects on the compressive behavior of closed-cell Al foam, Acta Mater. 53 (2005) 3415–3423.